Atmospheric Research 261 (2021) 105756

Contents lists available at ScienceDirect

Atmospheric Research

journal homepage: www.elsevier.com/locate/atmosres

The mechanism of the formation of high sulfate concentrations over the Yellow Sea during the KORUS-AQ period: The effect of transport/atmospheric chemistry and ocean emissions

Wonbae Jeon [a,b], Jaehyeong Park [c], Yunsoo Choi [d,*], Jeonghyeok Mun [b,c], Dongjin Kim [b,c], Cheol-Hee Kim [a,e], Hyo-Jung Lee [e], Juseon Bak [e], Hyun-Young Jo [e]

[a] Department of Atmospheric Sciences, Pusan National University, Busan 46241, South Korea
[b] BK21 School of Earth and Environmental System, Pusan National University, Busan 46241, South Korea
[c] Division of Earth Environmental System, Pusan National University, Busan 46241, South Korea
[d] Department of Earth and Atmospheric Sciences, University of Houston, Houston, TX 77204, USA
[e] Institute of Environmental Studies, Pusan National University, Busan 46241, South Korea

ARTICLE INFO

Keywords:
Sulfate
KORUS-AQ
CMAQ
Process analysis
Ocean emissions

ABSTRACT

This study investigates the chemical properties of high-concentration sulfate (SO_4^{2-}) that appeared on the surface of the Yellow Sea during the KORUS-AQ period (April–June 2016). For quantitative analysis, we carry out numerical simulation using the Community Multi-scale Air Quality (CMAQ) model for the KORUS-AQ period (the BASE case) and another simulation of ocean emissions (the OCEAN case) that determines the effect of including ocean emissions on the results of the analysis. CMAQ-simulated (the BASE case) sulfate (SO_4^{2-}), nitrate (NO_3^-), ammonium (NH_4^+), elemental carbon (EC), and organic carbon (OC) show high concentrations of these constituents centering around eastern China, the Liaodong Peninsula, and the western inland area of the Korean Peninsula. SO_4^{2-}, unlike the other particulate matter constituents, shows high concentrations (up to 14.44 $\mu g/m^3$) at the surface of the Yellow Sea. Results of the Integrated Process Rate (IPR) analysis show that the chemical production of SO_4^{2-} over the Yellow Sea can primarily be attributed to the "aerosol process", which is mainly dependent on weather conditions (e.g., temperature and wind speed) and concentrations of precursors such as SO_2 and OH. The results of the analysis of the mechanism of SO_4^{2-} formation using the Sulfur Tracking Model (STM) show that most chemical SO_4^{2-} production (79.12%) on the surface of the Yellow Sea is the result of the aqueous-phase chemical reactions following the SO_2 oxidation reaction ($OH + SO_2 \rightarrow H_2SO_4 + HO_2$). Comparing the results of the OCEAN and BASE cases, we find that the primary mechanism of SO_4^{2-} formation over the Yellow Sea shows no significant change with regard to ocean emissions. These results also confirm that increases in SO_4^{2-} concentrations (up to 4.79 $\mu g/m^3$) on the surface of the sea are not proportional to the distribution and amounts of ocean emissions, and in some areas, concentrations could decrease (up to −2.65 $\mu g/m^3$) as a result of complex non-linear chemical reactions.

1. Introduction

A major component of particulate matter ($PM_{2.5}$), sulfate (SO_4^{2-}) (Ho et al., 2003; Liu et al., 2020a, 2020b), accounts for the highest ratio of South Korean $PM_{2.5}$ among single components (Lee et al., 1999; Lee and Kang, 2001; Park et al., 2018). Concentrations of SO_4^{2-} in South Korea are affected by not only domestic air pollutant emissions but also the effects of transport from other countries (Kim et al., 2001; Lee et al., 2015; Bae et al., 2020a). Since ascertaining the transport mode is a complex task, accurately analyzing the characteristics of SO_4^{2-} and predicting changes in its concentrations are challenging. In South Korea, doing so requires an in-depth understanding of the complicated process of the chemical changes taking place when SO_4^{2-} and its precursors are transported from other counties to South Korea; hence, a number of researchers have actively studied the process in recent years.

Several studies (Lee et al., 2002; Kim et al., 2012; Cha et al., 2020; Jo et al., 2020) have reported that the measured SO_4^{2-} in a particular area of South Korea did not originate from domestic emission sources but

* Corresponding author.
E-mail address: ychoi6@uh.edu (Y. Choi).

https://doi.org/10.1016/j.atmosres.2021.105756
Received 17 March 2021; Received in revised form 23 May 2021; Accepted 29 June 2021
Available online 2 July 2021

instead from the long-range transport of air pollutants from eastern China. This finding was confirmed by Kim et al. (2001) in a study in which they analyzed aircraft measurement data and found that sulfur dioxide (SO_2) was converted into SO_4^{2-} during the long-range transport of air pollutants. Another study by Lee et al. (2015) identified a relationship between high-concentrations of SO_4^{2-} and SO_2 emitted from eastern China based on SO_4^{2-}, nitrate (NO_3^-), ammonium (NH_4^+), and organic matter data observed over Baengnyeongdo Island in South Korea from May to November 2011. Using the Aerodyne High-Resolution Time of Flight Aerosol Mass Spectrometer (HR-ToF-AMS), the authors of the study analyzed case studies on the potential source contribution function. A multi-year study of South Korean metropolitan areas by Bae et al. (2020a) analyzed the characteristics of changes in the concentrations of major $PM_{2.5}$ constituents, including SO_4^{2-}, quantitatively confirmed the effect of the long-range transport of air pollutants from China. A numerical study by Jung et al. (2021) reported that the concentrations of SO_4^{2-} and NH_4^+ on the Yellow Sea could increase due to aqueous chemistry when a temperature inversion layer is formed on foggy days.

Although these studies have significance, as they enabled researchers to estimate the contribution of external emission sources to domestic SO_4^{2-} concentrations through analyses focusing on a receptor, they did not elucidate the process of chemical changes that took place while the pollutants flowed from other countries into South Korea. To tackle these challenges, Jeon et al. (2018) analyzed the characteristics of the chemical reaction that occurs when SO_2 in the eastern China region is transported to South Korea over the Yellow Sea and quantitatively explained the mechanism of SO_4^{2-} formation over the Yellow Sea. The significance of this study is that it concretely explains why concentrations of SO_4^{2-} increase when it is transported from China to South Korea. This study, however, contains several limitations that preclude the accurate verification of simulated SO_4^{2-} concentrations over certain areas of the sea, and it does not account for ocean emissions in the analysis of the results.

In general, as observation sites over the sea surface are sparsely distributed, obtaining meaningful air quality measurement data (e.g., concentrations of each $PM_{2.5}$ component) is challenging. However, a joint air quality survey study by the South Korean Ministry of Environment and the U.S. National Aeronautics and Space Administration (Korea-United States Air Quality; KORUS-AQ) performed in 2016 enabled us to secure airborne observation data pertaining to $PM_{2.5}$ components of some areas of the Yellow Sea, located between China and South Korea. Accordingly, we were able to use the observation data to objectively evaluate the numerical simulation results of SO_4^{2-} concentrations on the surface of the Yellow Sea. Furthermore, we accessed information about marine pollutants in South Korean territorial waters from recent emissions data from South Korea; thus, we were able to account for ocean emissions in our air quality models, which indicates the possibility of the objective verification and additional analysis of the results of existing studies that relate to the characteristics of SO_4^{2-} formation and reduction over the sea surface.

With the data mentioned above, we numerically simulated the chemical changes that occur when SO_4^{2-} is transported from China to South Korea through the Yellow Sea. To that end, we use $PM_{2.5}$ surface observation data that cover all regions of China and South Korea, along with airborne observation data of the Yellow Sea, to achieve sufficient reliability of the SO_4^{2-} simulation results from the Community Multiscale Air Quality (CMAQ) model (Byun and Schere, 2006). Then we analyze the mechanism of the formation of high SO_4^{2-} concentrations on the surface of the Yellow Sea that appeared during the KORUS-AQ period from April to June 2016 and investigate the difference between the mechanisms reported by previous studies and those found in this study. We also examine the effect of ocean emissions on changes in the characteristics of SO_4^{2-} production and loss. Ultimately, we interpret these results comprehensively and offer more objective explanations for changes in SO_4^{2-} concentrations change over the Yellow Sea.

2. Methodology

2.1. Modeling system and data

This study applied the CMAQ (v5.0.2), a three-dimensional photochemical transport model developed by the U.S. Environmental Protection Agency (EPA) for air quality numerical simulation. The simulation domains were Domain 1 (D1), which includes East Asia, with a 27 km grid resolution (178 × 142), and Domain 2 (D2), which includes eastern China, the Yellow Sea, and South Korea (Fig. 1), with a 9 km grid resolution (166 × 199). We investigated the phenomenon in which air pollutants emitted from eastern China regions are transported to the Yellow Sea in these domains. After conducting the modeling of D1, we used the results as initial and boundary fields for the modeling of D2. The vertical grid for the simulation consisted of 35 layers, and the top layer on which was set to 100 hPa. For the meteorological input field for the CMAQ simulation, we carried out Weather Research and Forecasting (WRF, v3.8.1) (Skamarock and Klemp, 2008) simulation and used the Meteorology Chemistry Interface Processor (MCIP) to convert results into input data for CMAQ. Then we used 0.25° × 0.25° Final Operation Global Analysis (FNL) data by the National Centers for Environmental Prediction (NCEP) as initial and boundary data for the WRF simulation. The numerical simulation covered the period between 09:00 LST, April 30, 2016, and 09:00 LST, June 14, 2016, the KORUS-AQ period. The detailed settings applied to the meteorology and air quality modeling are presented in Tables S1 and S2 (in the supplement).

For the emissions of the CMAQ model, we used the Mosaic Asian anthropogenic emission inventory (MIX) 2010 (Kim et al., 2017; Li et al., 2017; Souri et al., 2017a, 2017b), emissions data for the Asia region, and Clean Air Policy Support System (CAPSS) 2016 (National Institute of Environmental Research (NIER), 2019), national emissions data of South Korea. MIX is the emission data used for the development of MICS-Asia emissions and designed to support the Model Inter-Comparison Study for an Asia (MICS-Asia) model comparative study and the Task Force on the Hemispheric Transport of Air Pollution (TF HTAP) project. MIX provides information on the emissions of SO_2, nitrogen oxide (NO_x), carbon monoxide (CO), non-methane volatile organic compounds (NMVOC), ammonia (NH_3), PM_{10}, $PM_{2.5}$, black carbon (BC), organic carbon (OC), and carbon dioxide (CO_2) at a 0.25° × 0.25° resolution. CAPSS, used with MIX, is emission data produced by the National Institute of Environmental Research (NIER) in South Korea to identify the effects of improvements in air quality resulting from air pollution-related policies. It estimates and provides annual information about the emissions of eight air pollutants—carbon monoxide (CO), NO_x, sulfur oxides (SO_x), total suspended particles (TSP), PM_{10}, $PM_{2.5}$, VOCs, and NH_3—emitted from the point, area, mobile, and ocean pollution sources. The ocean emissions in the CAPSS emissions data include the information of emission sources from both areas near trading ports, with frequent arrival and departure of ships and all South Korean territorial waters apart from automobiles, railways, and aircraft. The ocean emissions of SO_2 (i.e., a major precursor of SO_4^{2-}) account for an estimated 3.3% (Table S3) of all South Korean emissions. For this study, we conducted the CMAQ simulation on the BASE case, in which we did not account for ocean emissions in the CAPSS 2016 emissions data, and the OCEAN case, in which we did account for the data. Once we identified the difference between the concentrations of SO_2 of the two cases from the results of the simulation, we analyzed the characteristics of changes in the concentrations of SO_4^{2-}.

2.2. Surface and airborne measurements

For the quantitative evaluation of the CMAQ modeling results, we collected data from 408 sites at Air Quality Monitoring Stations (AQMS), provided by NIER in South Korea, and air quality observation data from 1433 sites provided by the Ministry of Environmental Protection in China (Fig. 1). The AQMS of South Korea provides measured

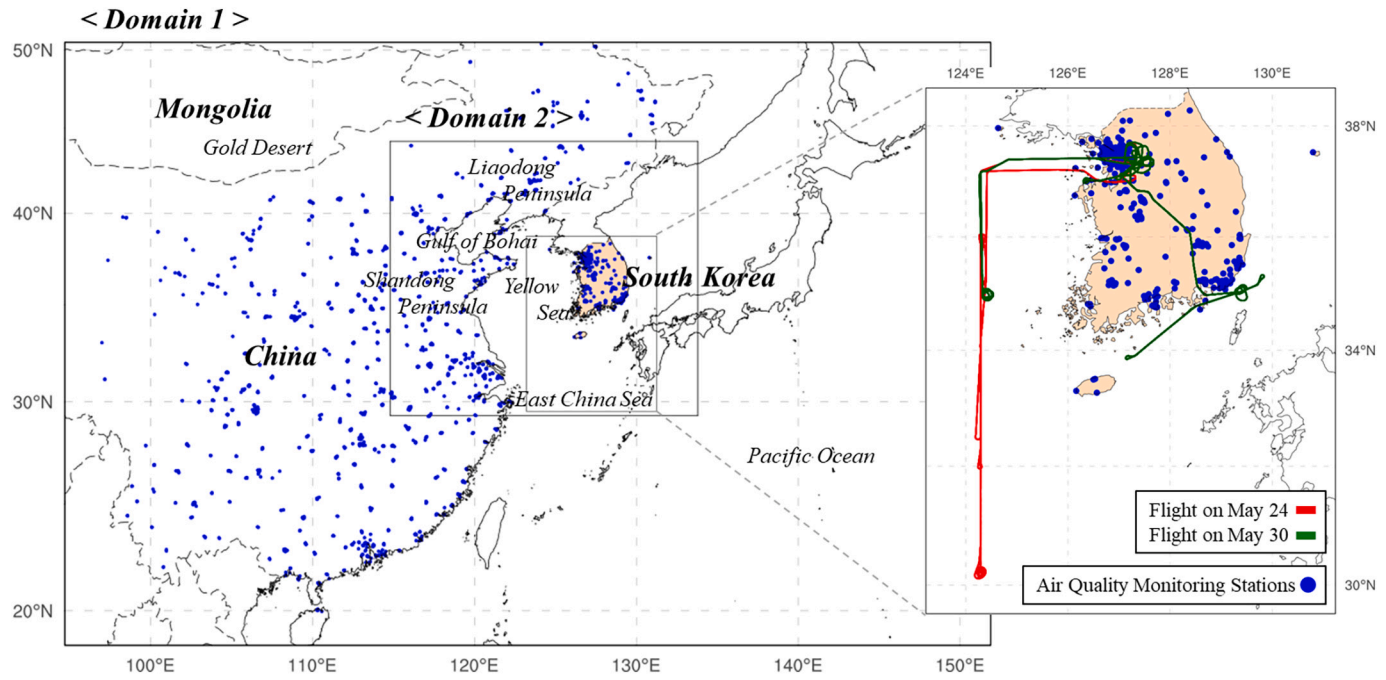

Fig. 1. The distribution of air quality observation points within the numerical simulation domain and the simulated area of the WRF and CMAQ models (blue dots). The lines in the right panel present the DC-8 aeronautical observation pathways on May 24 (red) and May 30 (green) during the KORUS-AQ period. (For interpretation of the references to colour in this figure legend, the reader is referred to the web version of this article.)

concentrations of PM_{10}, $PM_{2.5}$, ozone (O_3), SO_2, NO_2, and CO on the surface at a one-hour time interval, and the air quality observation data of China provides concentrations of PM_{10}, $PM_{2.5}$, O_3, SO_2, NO_2, and CO on the surface along with daily average air quality index values also at a one-hour time interval. In this study, we used the hourly $PM_{2.5}$ concentration observation data of South Korea and China to evaluate the simulation results of surface $PM_{2.5}$. In addition, we used DC-8 aircraft observation data during the KORUS-AQ period to evaluate the simulation results of the SO_4^{2-} concentrations over the Yellow Sea. The DC-8 is a research aircraft of NASA in the United States and observes aerosols, water vapor, and winds with a mounted weather environment sensor. It provided 22 separate measurements over the Yellow Sea from May 2 to June 10 during the KORUS-AQ period (Peterson et al., 2019; Simpson et al., 2020). We used the DC-8 measurement data on May 24 and May 30, when flights over the Yellow Sea took place, to evaluate the results of the CMAQ simulation of SO_4^{2-}.

2.3. Quantitative analysis based on IPR and STM

To analyze the processes that contributed to high concentrations of SO_4^{2-} that occurred on the surface of the Yellow Sea, we used the integrated process rate (IPR) module, provided in the CMAQ model, and the sulfur tracking model (STM) (Li et al., 2014; Fan et al., 2015; Pan et al., 2015, 2017; Itahashi et al., 2018; Jeon et al., 2018). The IPR estimates the relative contributions of individual physical and chemical processes to each type of process (e.g., transport, emission, deposition, cloud, and aerosol process) of pollutants. The STM is a selective diagnostic model included in CMAQ v5.0.2 that quantitatively estimates the contributions of the chemical reaction of the gas- and aqueous-phases to the total amount of SO_4^{2-}, along with emissions, initial conditions, and boundary conditions. A summary of the total number of reactions that contribute to the formation of SO_4^{2-} is listed in Table 1. For this study, we compared the concentrations of each reaction to the total amount of SO_4^{2-} and analyzed the contribution of each reaction.

Table 1
Chemical reactions related to the formation of SO_4^{2-} simulated by the CMAQ-STM model.

Reaction	Description
$OH + SO_2 \rightarrow H_2SO_4 + HO_2$	SO_4^{2-} production by nucleation and/or condensation following the SO_2 oxidation reaction ($OH + SO_2 \rightarrow H_2SO_4 + HO_2$)
$H_2O_2 + S(IV) \rightarrow S(VI) + H_2O$	SO_4^{2-} production by an aqueous-phase H_2O_2 oxidation reaction
$O_3 + S(IV) \rightarrow S(VI) + O_2$	SO_4^{2-} production by an aqueous-phase O_3 oxidation reaction
$O_2 + S(IV) \rightarrow S(VI)$	SO_4^{2-} production by an aqueous-phase O_2 oxidation reaction
$MHP + S(IV) \rightarrow S(VI)$	SO_4^{2-} production by an aqueous-phase MHP oxidation reaction
$PAA + S(IV) \rightarrow S(VI)$	SO_4^{2-} production by an aqueous-phase PAA oxidation reaction

*MHP: methyl hydrogen peroxide; **PAA: peroxyacetic acid.

2.4. Statistical parameters

In this study, we referred to the statistical indices proposed in various previous studies, such as the index of agreement (IOA), the mean bias error (MBE), the normalized mean bias error (NBE), and the mean fractional bias (MFB) (Willmott et al., 1985; Hurley et al., 2001; Boylan and Russell, 2006; Emery et al., 2017) to quantitatively evaluate the results of the air quality simulation. The definition of each index is tabulated in Table 2. According to previous studies that assess the accuracy of a $PM_{2.5}$ simulation by the air quality model, if the NMB is ±30% (Emery et al., 2016) and the IOA is exceeding 0.5 (Hurley et al., 2001; Willmott et al., 1985), the modeling results are determined to appropriately explain the phenomenon; and if the NMB is within ±10%, they are determined to show superior performance (Emery et al., 2016). In terms of the MFB, we used the goal ($\leq 1.7e^{-2\overline{C}} + 0.3$) value and criteria ($\leq 1.4e^{-2\overline{C}} + 0.6$) value proposed by Boylan and Russell (2006) to determine if the simulated results satisfy the standard values.

Table 2
Statistical parameters and calculation formulas used for the quantitative evaluation of the meteorology and air quality simulation. N is the number of total compared points, P_i is the CMAQ simulated value, $\overline{P}$ is the CMAQ simulation mean, O_i is the observed value, $\overline{O}$ is the observation mean, and $\overline{C}$ is $\left(\overline{P}+\overline{O}\right)/2$.

Statistical parameter	Formula
Index of Agreement (IOA)	$\mathrm{IOA} = 1 - \frac{\sum_{i=1}^{N}(P_i - O_i)^2}{\sum_{i=1}^{N}\left(\left\|P_i - \overline{P}\right\| + \left\|O_i - \overline{O}\right\|\right)^2}$
Mean Bias Error (MBE)	$\mathrm{MBE} = \frac{\sum_{i=1}^{N}(P_i - O_i)}{N}$
Normalized Mean Bias (NMB)	$\mathrm{NMB} = \frac{\sum_{i=1}^{N}(P_i - O_i)}{\sum_{i=1}^{N}(O_i)} \times 100$
Mean Fractional Bias (MFB)	$\mathrm{MFB} = \frac{2}{N}\sum_{i=1}^{N}\frac{P_i - O_i}{P_i + O_i}$
	$\lvert\mathrm{MFB\ (goals)}\rvert \le 1.7e^{-2\overline{C}} + 0.3$
	$\lvert\mathrm{MFB\ (criteria)}\rvert \le 1.4e^{-2\overline{C}} + 0.6$

3. Results and discussion

3.1. Model performance evaluation

3.1.1. Air quality simulation evaluation based on the surface observation data

Using the statistical parameters shown in Section 2.4, we evaluated the results of the surface $PM_{2.5}$ concentration simulation from April 30, 2016 to June 14, 2016. Fig. 2-(a) shows the scatterplot of $PM_{2.5}$ simulated concentrations (BASE case) and surface observation data and statistical analysis results. Although the results of the CMAQ simulation, compared with the observed values, slightly under-estimated concentrations(MBE: −2.72), they showed an IOA exceeding 0.7 (IOA: 0.72) and an NMB within ±10% (NMB: −7.59%), suggesting that the simulated results could reproduce the temporal variation of $PM_{2.5}$; furthermore, the deviation of the results was not significant. The MFB value of the $PM_{2.5}$ simulation results of the CMAQ was 0.245 (Fig. 2-(b)), which satisfies the goal standard $\left(\le 1.7e^{-2\overline{C}} + 0.3\right)$ proposed by Boylan and Russell (2006), indicating that the results of the $PM_{2.5}$ simulation results were very close to the observed values.

Fig. 3 presents the horizontal distribution of the mean $PM_{2.5}$ simulation and observation results during the simulation period. As shown in the figure, the CMAQ simulation expresses the distribution of high concentrations of $PM_{2.5}$ centering around eastern China and several areas in South Korea, along with the distribution of relatively low

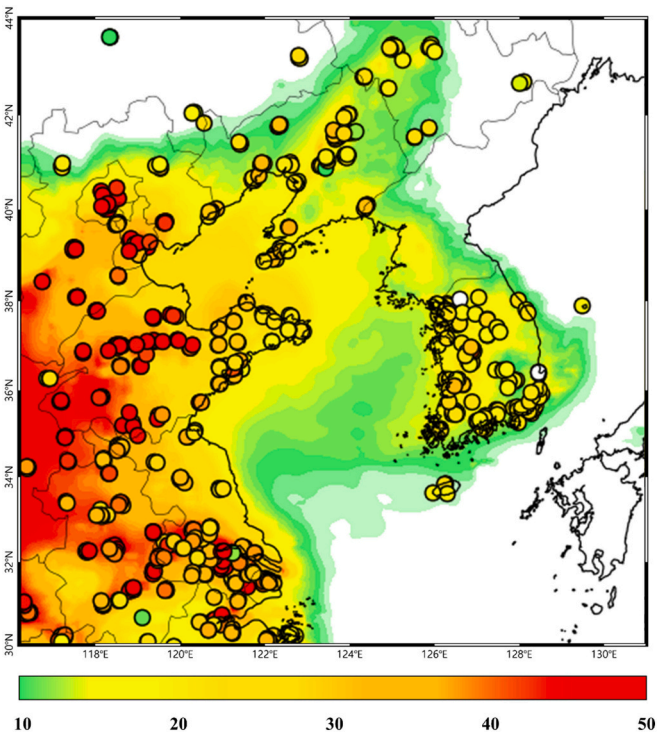

Fig. 3. The horizontal distribution of surface $PM_{2.5}$ concentrations simulated by CMAQ (the BASE case) and the $PM_{2.5}$ observation concentrations of all surface observation sites in the domain (colored circles). Each value represents the mean of the entire simulation period.

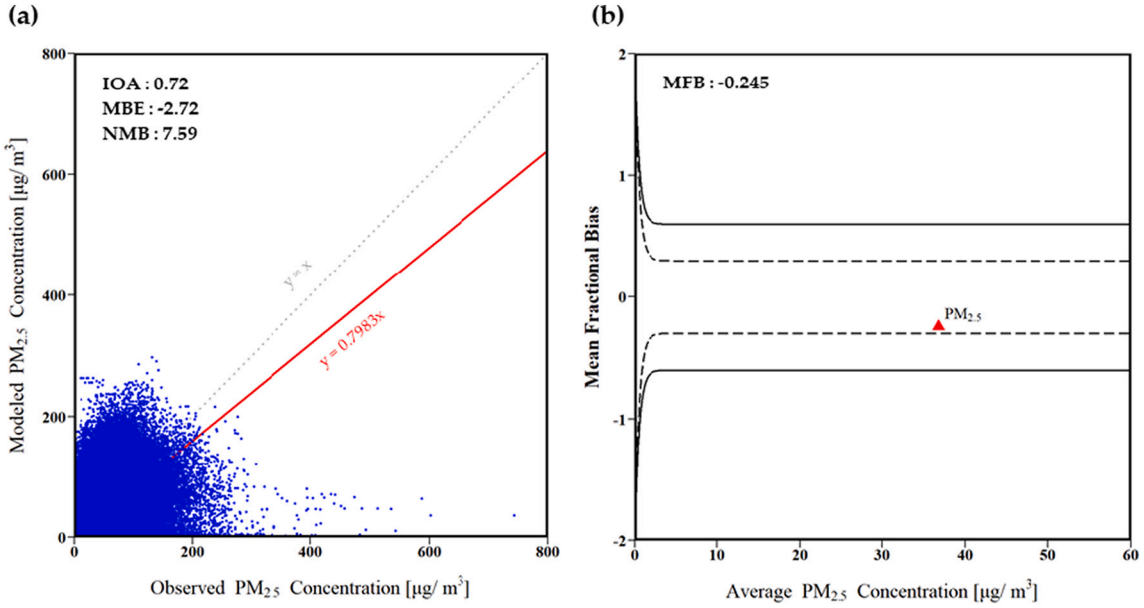

Fig. 2. (a) Scatter plot of CMAQ-simulated $PM_{2.5}$ concentrations (BASE case) and surface observation concentrations and (b) the results of the mean fractional bias (MFB) analysis of the entire simulation period (April 30–June 14, 2016). The lines presented in the MFB analysis results are the standards suggested by Boylan and Russell (2006); the solid lines represent the criteria and the dotted lines the standard of the goal.

concentrations of $PM_{2.5}$ in northeastern China and areas near Mongolia close to the observed values.

3.1.2. Validation of the SO_4^{2-} simulation results using DC-8 aircraft measurement data

For the quantitative evaluation of SO_4^{2-} concentrations on the surface of the Yellow Sea simulated by CMAQ, we used the DC-8 aircraft measurement data to carry out an additional verification. The DC-8 aircraft measured SO_4^{2-} concentrations on two days (May 24 and May 30), when the south-north directional flight over the eastern part of the Yellow Sea (Fig. 1) occurred during the KORUS-AQ period, and we compared them with the CMAQ simulation results.

As presented in Fig. 4, the two cases from May 24 and 30 and the CMAQ simulation results close agreed with the observation results. The variation among the SO_4^{2-}concentrations with changes in the time and the altitude was also successfully simulated. The results from May 30 (Fig. 4-(b)) indicate that the SO_4^{2-} concentration near the surface at 13:00–15:00 LST, when the flight path of the DC-8 was above the southeastern coast of South Korea, was over-estimated by CMAQ (Fig. 1). Because ports are densely located and the movement of ships is considerable in this region, the distribution of ship emissions is significant. Owing to the uncertainty of these ship emissions (mostly the precursor of SO_4^{2-}, i.e., SO_2), we analyzed them to determine whether they led to the difference between the CMAQ simulation results and the observed values. The CMAQ simulation results, however, were similar to the observed values in general, indicating that the results of the SO_4^{2-} simulation were reliable. Thus, we deemed the results of the model suitable for the analysis of the SO_4^{2-} production, loss, and transport processes over the Yellow Sea during the KORUS-AQ period.

3.2. Increase in SO_4^{2-} concentrations at the sea surface during transport

On the basis of the validated CMAQ simulation results, we investigated the characteristics of the distribution of SO_4^{2-} concentrations over the Yellow Sea during the KORUS-AQ period and then compared them with other $PM_{2.5}$ constituents. Fig. 5 shows the mean distribution of SO_4^{2-} concentrations over the Yellow Sea (during the KORUS-AQ period) and surrounding areas. The figure also presents a comparison of concentrations of other $PM_{2.5}$ constituents; NO_3^-, NH_4^+, elemental carbon (EC), primary organic carbon (POC), and secondary organic carbon (SOC).

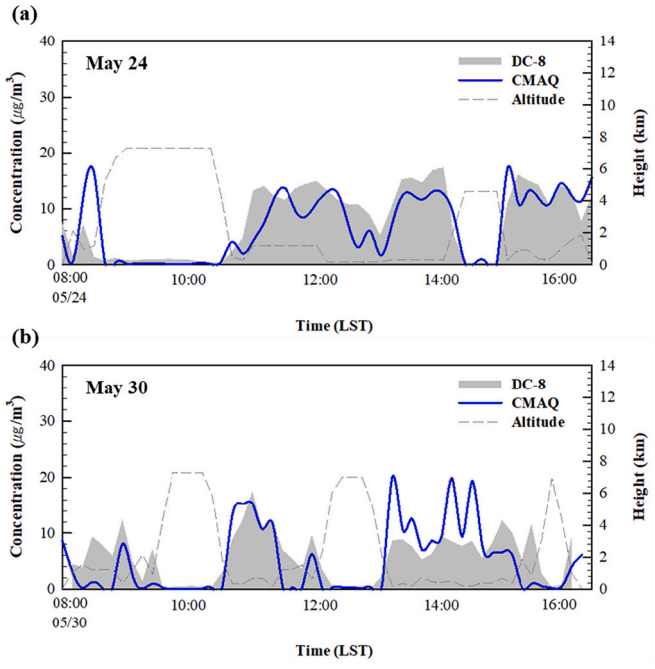

Fig. 4. Time series of SO_4^{2-} concentrations measured by DC-8 aircraft measurements performed on (a) May 24 and (b) May 30 (gray shade) and the CMAQ SO_4^{2-} simulation concentration (blue line). The gray dotted line shows changes in the altitude of the DC-8 aircraft each hour. (For interpretation of the references to colour in this figure legend, the reader is referred to the web version of this article.)

In terms of the distribution of the above constituents, we found high concentrations centering around eastern China, the Liaodong Peninsula, and the west inland area of the Korean Peninsula. Because of the distribution of a large number of emissions in the regions, this finding is understandable (Guan et al., 2014; Bae et al., 2020b). Interestingly, however, the distribution of SO_4^{2-} concentrations at the surface of the Yellow Sea showed distinct characteristics from those of the other constituents. Although concentrations of pollutants on the sea surface are generally lower than those on inland area surfaces because of the more limited distribution of emissions on the sea surface (Pozzoli et al., 2011), SO_4^{2-} concentrations at the surface of the Yellow Sea during the simulation period were as high as 14.44 $\mu g/m^3$,exceeding concentrations over inland areas of the Korean Peninsula and northeastern China. The high concentrations in the Yellow Sea were found only in the results of SO_4^{2-}, and not in the results of other substances such as NO_3^-, NH_4^+, EC, and OC (POC + SOC). The results of this study confirm the occurrence of the phenomenon of high SO_4^{2-} concentrations at the surface of the Yellow Sea reported in several previous studies (Itahashi et al., 2012; Jeon et al., 2018) during the KORUS-AQ period.

To identify the characteristics of high SO_4^{2-} concentrations at the surface of the Yellow Sea, we conducted a comparative analysis of the distribution of daily SO_4^{2-} concentrations during the entire simulation period. Based on the results of the analysis results, we confirmed that high concentrations of SO_4^{2-} appeared at the sea surface on most simulation days, in particular, from May 29 to June 1, when SO_4^{2-} concentrations were higher than those in most inland areas. This phenomenon, however, was not captured for the other constituents (Fig. 6-(a)). Therefore, we selected the May 29 to June 1 period (Episode Period; "EP") for intensive, detailed analysis of the formation process of high-concentration SO_4^{2-} at the surface of the Yellow Sea.

3.3. Analysis of the SO_4^{2-} high-concentration mechanism at the surface of the Yellow Sea

To investigate the mechanism of high-concentration SO_4^{2-} formation during the EP (May 29–June 1), we conducted a quantitative analysis using the IPR and the STM. During the EP period, we analyzed and averaged the concentrations at an altitude below 1 km, where SO_4^{2-} was mostly distributed at the surface of the Yellow Sea (Fig. S1).

Fig. 7 shows the results of the IPR analysis of the EP and presents changes in the SO_4^{2-} concentrations on each day of the EP and the concentrations contributed by each process in the region where changes in SO_4^{2-} concentrations at the surface of the Yellow Sea were most distinctly captured (hereafter, "YS") (Fig. 6). The results of May 29 (Day 1) (i.e., the first day of the EP) show increases in SO_4^{2-} concentrations from 09:00 LST, when the contribution of "horizontal transport" becomes apparent (up to 0.17 $\mu g/m^3/h$). That is, the high concentration of SO_4^{2-} that appeared on Day 1 was mainly attributed to horizontal transport. The analysis showed that SO_4^{2-} over eastern China (mostly near the Shandong Peninsula) was introduced to the Yellow Sea in a clockwise direction following the Gulf of Pohai and the western area of the Korean Peninsula (Fig. S2), causing the high concentrations of SO_4^{2-}; hence, the effect of chemical formation on high concentrations of SO_4^{2-} on Day 1 is limited.

On May 30 (Day 2), SO_4^{2-} concentrations increased from 08:00 LST (right after sunrise), and unlike on Day 1, the increase in the "aerosol process" became noticeable (up to 0.12 $\mu g/m^3/h$). This finding suggests that the high concentration of SO_4^{2-} on Day 2 could not simply be attributed to horizontal transport but to chemical formation at the

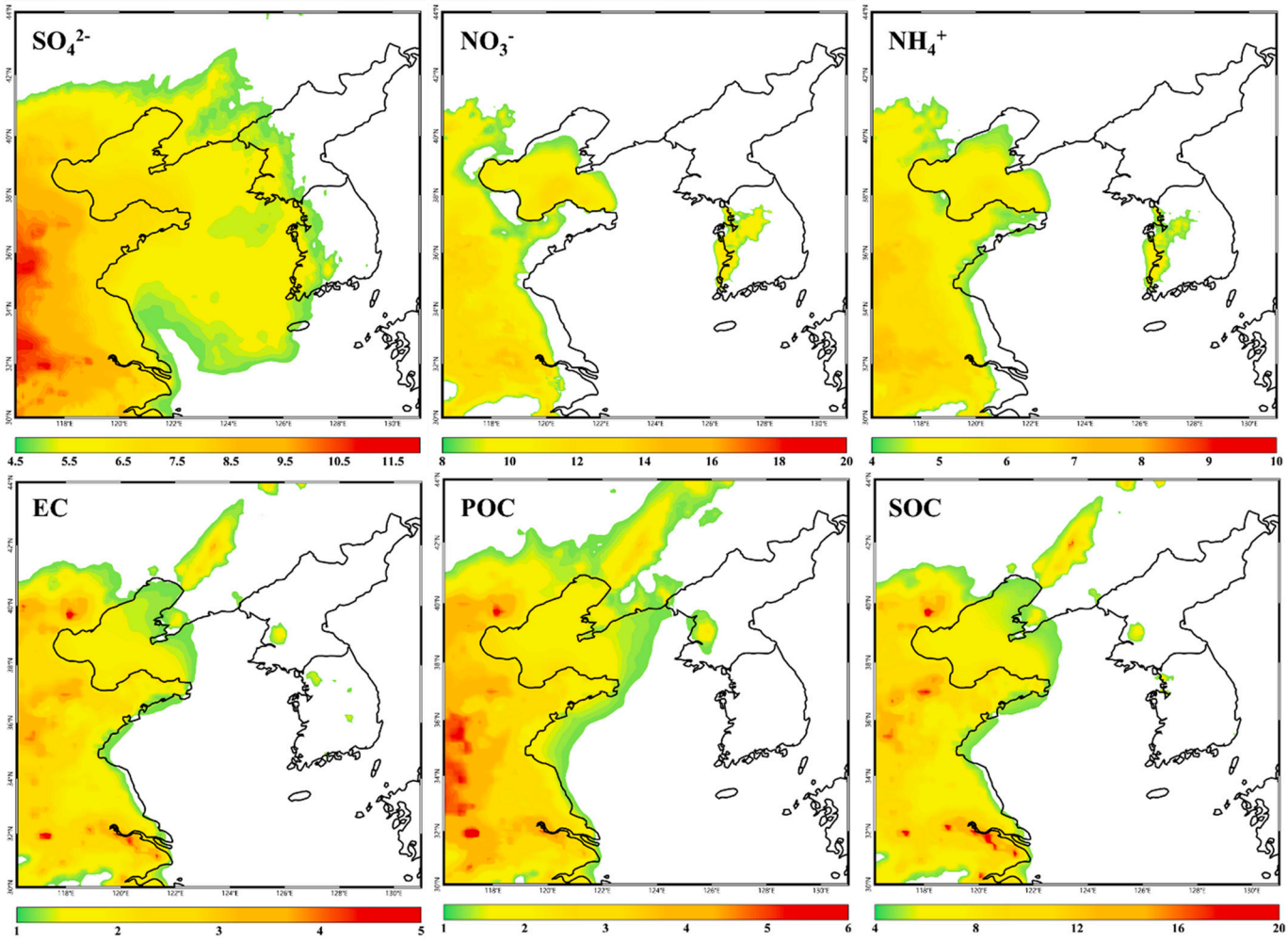

Fig. 5. The horizontal distribution of the concentration of SO_4^{2-}, NO_3^-, NH_4^+, EC, POC, and SOC simulated by CMAQ. Each value represents the average of the grid values with an altitude of below 1 km during the entire simulation period.

surface of the sea. The increase in SO_4^{2-} concentrations on Day 2 was mainly due to chemical SO_4^{2-} production by aerosol process and its vertical mixing resulting from thermal and mechanical momentum transport.

To investigate the detailed chemical mechanism causing the increase in SO_4^{2-} concentrations on Day 2, we carried out an STM analysis. As presented in Table 3, most of the chemical SO_4^{2-} production on Day 2 (4.16 $\mu g/m^3$, 79.07%) was attributed to the aqueous-phase chemical reactions following the SO_2 oxidation reaction by OH (i.e., $OH + SO_2 \rightarrow H_2SO_4 + HO_2$) (Table 1). This finding is consistent with that by Jeon et al. (2018), who provided an explanation for the high concentrations of SO_4^{2-} on the Yellow Sea during the winter. The finding also shows that during the KORUS-AQ period, which corresponds to the spring, the phenomenon of high-concentration SO_4^{2-} resulted from the chemical reaction of SO_2 transported to the Yellow Sea. In the case mentioned above, however, Jeon et al. (2018) reported that SO_2 was directly introduced to the Yellow Sea from eastern China, while our study found that it was introduced to the western area of the Korean Peninsula following its flow in a clockwise direction. This difference suggests that SO_2 emissions from not only eastern China but also inland areas of the Korean Peninsula could contribute to the production of high-concentration SO_4^{2-} at the surface of the Yellow Sea.

On May 31 (Day 3), similar to Day 2, the concentrations of SO_4^{2-} increased from 08:00 LST (right after the sunrise) on and the analysis showed that the increase was mainly due to the "aerosol process" (up to 0.08 $\mu g/m^3/h$). The concentration was higher on Day 3 (5.47 $\mu g/m^3$) than it was on Day 2 (4.16 $\mu g/m^3$) because concentrations produced on Day 2 continued to increase in the YS region. Most production of the chemical SO_4^{2-} on Day 3 (85.95%) was also attributed to the SO_2 oxidation reaction by OH, similar to the findings on Day 2. The concentration of SO_4^{2-} produced by the "aerosol process" on Day 3 (up to 0.08 $\mu g/m^3/h$), however, was lower than that on Day 2 (up to 0.12 $\mu g/m^3/h$). To explain this finding, we compared the weather conditions on the two case days (Days 2 and 3). When the temperature was high and the radiation strong, SO_4^{2-} was well-formed (Requia et al., 2019); and as less dispersion and transport took place when the wind speed was low, conditions for the formation of SO_4^{2-} were ideal. Table 4 presents the temperature and the wind speed, the major meteorological factors related to the production of chemical SO_4^{2-} on each case day. The table shows that the temperature on Day 3, which was higher than it was on Day 2, and the wind speed, which was lower, were relatively more favorable to the production of SO_4^{2-}. Despite the relatively favorable weather conditions, the SO_4^{2-} produced by the "aerosol process" on Day 3 was lower than that on Day 2. This finding implies that the differences between the results of the two case days cannot simply be attributed to the difference in weather conditions.

In addition to comparing weather conditions, we compared the concentrations of the major precursors of SO_4^{2-} (i.e., SO_2 and OH). As shown in Table 3, most of the SO_4^{2-} production over the Yellow Sea was due to the SO_2 oxidation reaction by OH; hence, we compared the concentrations of SO_2 and OH on the two days (Days 2 and 3) to the concentrations of SO_4^{2-} of those days. As can be seen in Fig. 8, while the

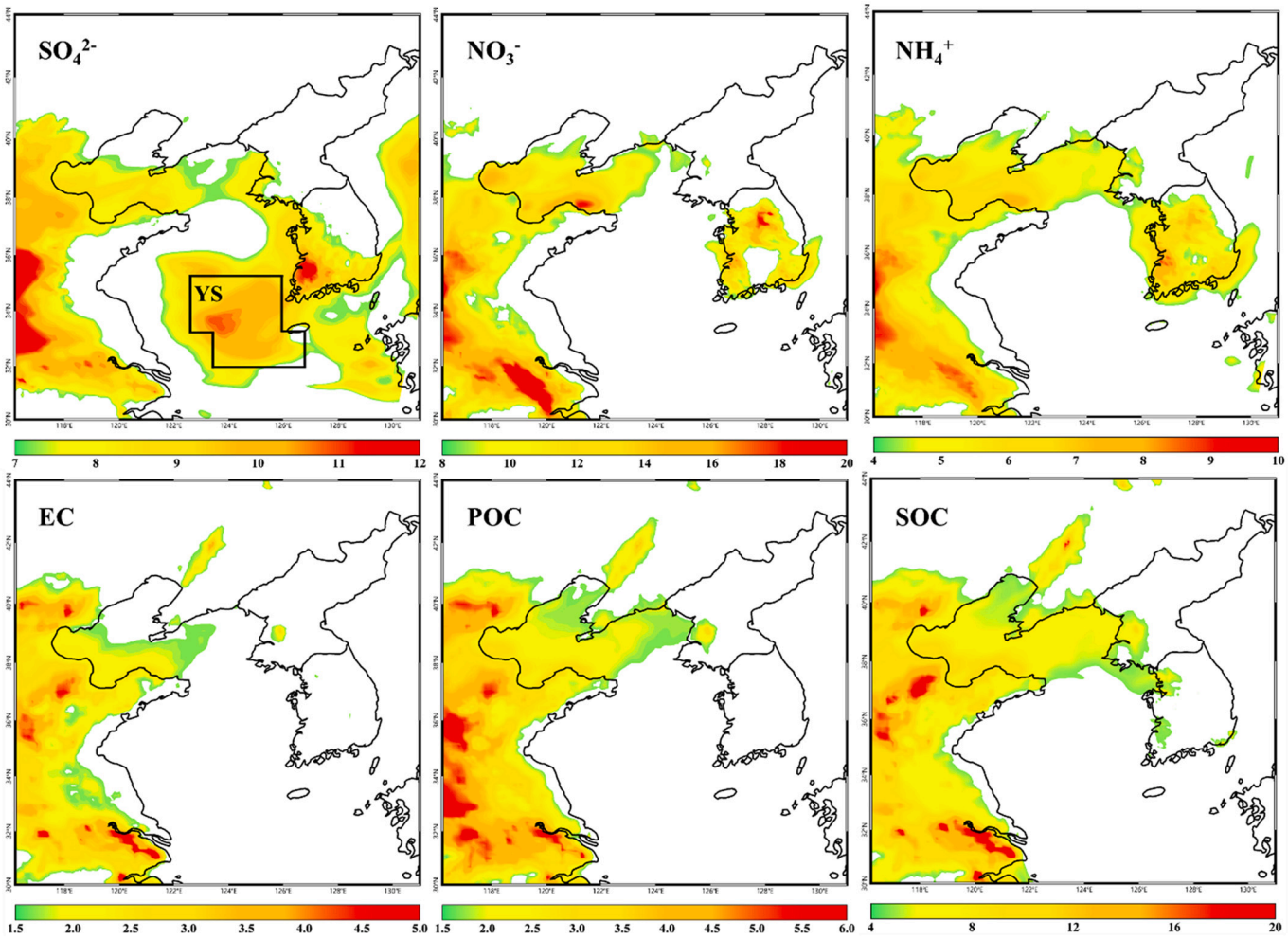

Fig. 6. The same as in Fig. 5, but for May 29–June 1. The boxed area denotes the SO_4^{2-} high-concentration region (YS) over the Yellow Sea, used for the IPR and STM analyses. (For interpretation of the references to colour in this figure legend, the reader is referred to the web version of this article.)

mean concentration of SO_2 on Day 3 was 9% higher than it was on Day 2, the concentration of OH was 74% lower on Day 3 than on Day 2. This finding indicates that the lower production of SO_4^{2-} attributed to the "aerosol process" on Day 3 than on Day 2 was the result of the lower OH concentrations (which are directly related to the oxidation reaction of SO_2). In their study, Jeon et al. (2018) asserted that the chemical production of SO_4^{2-} at the surface of the Yellow Sea is mainly dependent on weather conditions. According to the findings of this study, however, concentrations of SO_2 and OH required for the SO_2 oxidation reaction, together with weather conditions, are responsible for the production of SO_4^{2-} over the Yellow Sea.

Unlike on the previous days, on the last day, June 1 (Day 4), the concentration of SO_4^{2-} decreased because of the "cloud process". On Day 4, a monsoon front that had settled in the East China Sea moved north to the Yellow Sea, resulting in an increase in the cloud cover and the introduction of a large amount of water vapor (Fig. S3). As a result, the wet scavenging of SO_4^{2-} increased and the concentration decreased as much as $-0.44\ \mu g/m^3/h$.

These results imply that water vapor in the atmosphere may promote SO_4^{2-} production by chemical reactions but may also reduce SO_4^{2-} concentration by wet scavenging. To compare the difference in SO_4^{2-} concentration according to changes in water vapor mixing ratio (QV), additional CMAQ simulations were performed. Table 5 shows the change in SO_4^{2-} concentration with increasing QV. When QV increased by 10% (i.e., QV_1.1), the concentration of SO_4^{2-} increased by 3.71%, and the more QV increased, the larger the increase in SO_4^{2-} concentration. However, when QV increased by more than 60% (i.e., QV_1.6), the increase in SO_4^{2-} concentration no longer increased but rather decreased. This result reveals that water vapor in the atmosphere can enhance the chemical production of SO_4^{2-} by promoting its hygroscopic growth, but water vapor above a certain level might lead to reduced SO_4^{2-} concentration by wet deposition rather than chemical production. However, the effect of water vapor on SO_4^{2-} formation at sea could depend on the concentration of background substances, weather conditions, and so on. Also, since various processes affecting the chemical formation of SO_4^{2-} have been introduced in recent studies (Liu et al., 2020a, 2020b; Zhang et al., 2021; Wang et al., 2021), it is believed that continuous follow-up studies considering these factors will be required to fully understand the mechanism of sulfate production/loss at the Yellow Sea.

In summary, the production of chemical SO_4^{2-} on the surface of the Yellow Sea resulting from the SO_2 oxidation reaction takes place not only in the winter but also in the spring (the KORUS-AQ period). Furthermore, it is expected that the pathways to which SO_2 is introduced to the Yellow Sea are not always consistent but instead are dependent on the differences in seasonal pressure patterns. Generalizing these results, however, will entail additional analysis of a variety of cases, including those during the summer and the fall.

3.4. Effect of ocean emissions

On the basis of the previous analysis, we have determined that the

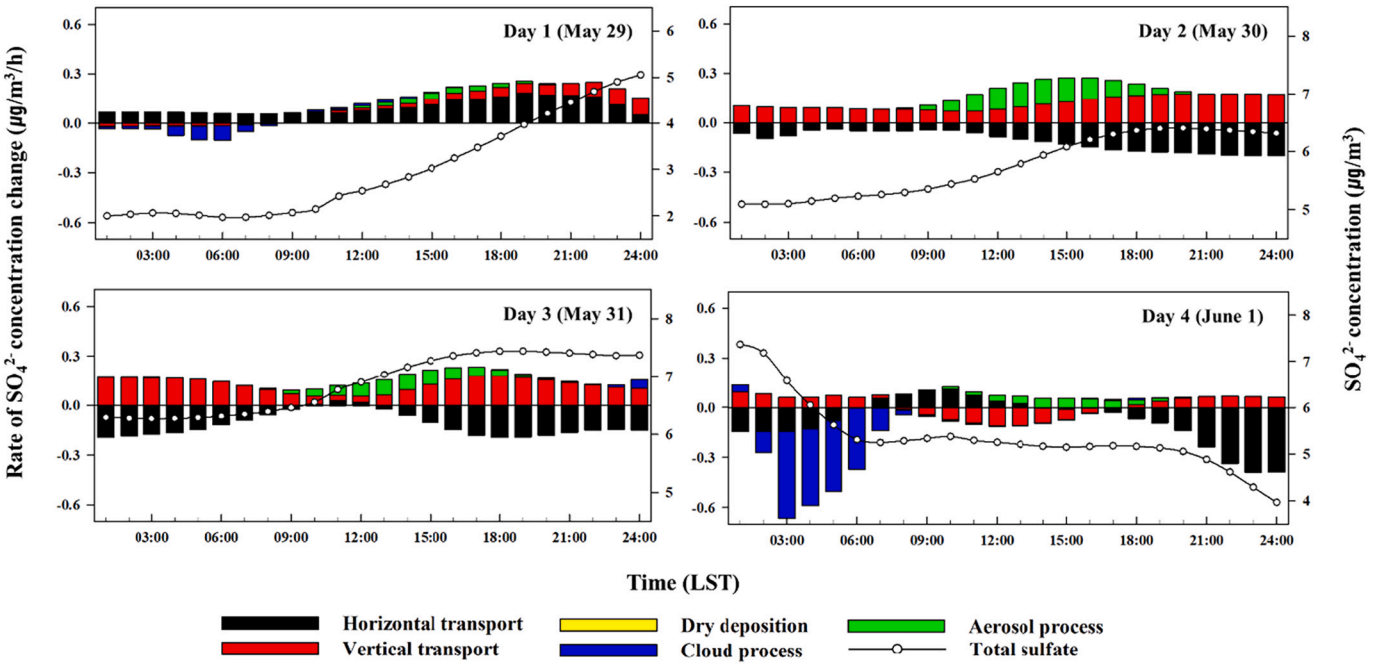

Fig. 7. The IPR analysis results (the BASE case) of the YS region during the EP (May 29–June 1). Each boxplot shows the amount of production and/or loss of SO_4^{2-} because of transport, deposition, and aerosol processes, and the line plot presents the SO_4^{2-} concentrations during the analysis period.

Table 3
Contributions of each chemical reaction to concentrations of SO_4^{2-} in the YS region on Day 2 (May 29) and Day 3(May 30), which are calculated by the STM. Each concentration value is the daily mean in the unit of μg/m^3; the value in parentheses indicates the percentage (%) of the total.

	Day 2		Day 3	
	BASE	**OCEAN**	**BASE**	**OCEAN**
$OH + SO_2 \rightarrow H_2SO_4 + HO_2$	4.16 (79.07)	4.19 (79.16)	5.47 (85.86)	5.51 (85.94)
$H_2O_2 + S(IV) \rightarrow S(VI) + H_2O$	1.05 (20.03)	1.06 (19.95)	0.86 (13.45)	0.86 (13.38)
$O_3 + S(IV) \rightarrow S(VI) + O_2$	0.00 (0.08)	0.00 (0.07)	0.00 (0.07)	0.00 (0.07)
$O_2 + S(IV) \rightarrow S(VI)$	0.00 (0.08)	0.00 (0.07)	0.00 (0.06)	0.00 (0.05)
*MHP + S(IV) → S(VI)	0.01 (0.10)	0.01 (0.10)	0.01 (0.08)	0.01 (0.08)
**PAA + S(IV) → S(VI)	0.03 (0.65)	0.03 (0.64)	0.03 (0.49)	0.03 (0.48)

*MHP: methyl hydrogen peroxide; **PAA: peroxyacetic acid.

Table 4
Daily average temperature and wind speed in the YS region during the EP (i.e., May 29 (Day 1)-June 1 (Day 4)).

	Day 1	Day 2	Day 3	Day 4
Temperature (°C)	9.08	9.21	9.49	9.49
Wind speed (m/s)	2.05	2.00	1.25	2.03

chemical production and loss of SO_4^{2-} over the Yellow Sea are mostly determined by the oxidation reaction of SO_2 and cloud process and that concentrations of SO_4^{2-} depends on the weather conditions on a particular case day and the concentration of precursors. However, we have based these research results assuming a complete lack of ocean emissions, which requires an additional analysis of how the mechanism of SO_4^{2-} formation over the Yellow Sea changes when ocean emissions are included. To this end, we set up an OCEAN case by adding ocean emissions to the BASE case, conducted an additional simulation using the CMAQ model, and analyzed the difference between the results of the two cases.

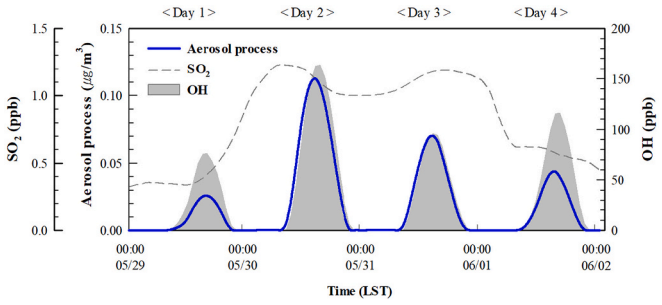

Fig. 8. Time series of the concentrations of SO_2 and OH and the rate of SO_4^{2-} production resulting from the "aerosol process" for the EP (May 29–June 1).

Fig. 9 presents the results of the IPR analysis of the OCEAN case. On May 29 (Day 1), the first day of the EP, SO_4^{2-} concentrations increased because of the "horizontal transport" process, similar to the BASE case (by as much as 0.17 μg/m^3/h). We attribute this increase to that the transport of pollutants emitted from eastern China and the western area of the Korean Peninsula to the YS region following a clockwise flow, as analyzed in Section 3.3. Results of the IPR analysis of May 30 and May 31 (Days 2 and 3) also indicate that the SO_4^{2-} concentration increased because of the "aerosol process", similar to the BASE case. From the results of the quantitative analysis of the difference between the concentrations formed through the "aerosol process" of the two cases (within the YS region), we identified the formation of more SO_4^{2-} in the OCEAN case from sunrise to sunset (Fig. 10). The difference between the concentrations of the two cases (the OCEAN case minus the BASE case) was likely due to the increase in SO_2 emissions among the constituents that comprise ocean emissions.

To investigate which chemical reaction mainly contributes to the increase in SO_4^{2-} concentrations by ocean emissions, we conducted an STM analysis on the OCEAN case. As presented in Table 3, of the total production of chemical SO_4^{2-} in the OCEAN case on Days 2 and 3, we found that the SO_2 oxidation reaction by OH (i.e., $OH + SO_2 \rightarrow H_2SO_4 + HO_2$) to be the highest at 79.16% (Day 2), and 85.94% (Day3). In other words, the formation of SO_4^{2-} was mainly the result of the SO_2 oxidation

Table 5
Changes in the simulated SO_4^{2-} concentration according to differences in water vapor mixing ratio (QV). The values are average in the YS region during the EP (May 29–June 1).

	BASE	QV_1.1	QV_1.2	QV_1.3	QV_1.4	QV_1.5	QV_1.6
SO_4^{2-} concentration ($\mu g/m^3$)	5.93	6.15	8.40	9.46	9.74	9.74	9.70
Rate of SO_4^{2-} increase (%)	–	3.71	41.65	59.53	64.25	64.25	63.58

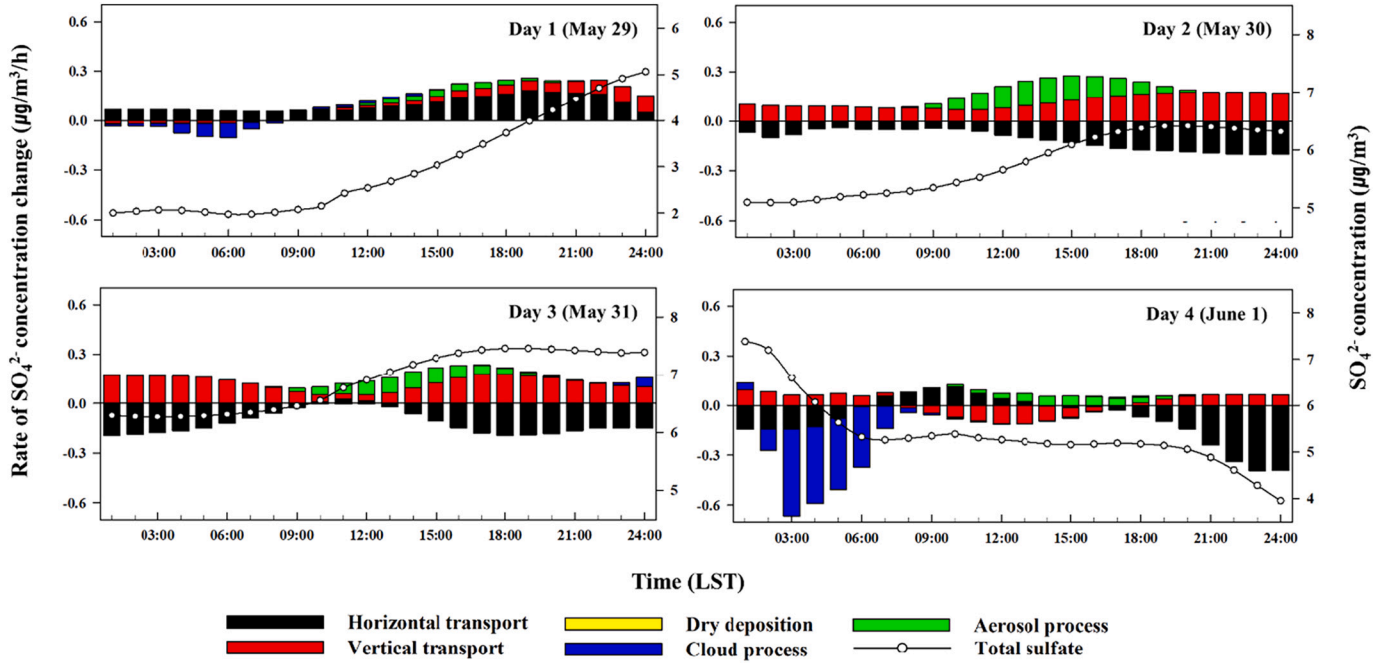

Fig. 9. The same as in Fig. 7, but for the OCEAN case.

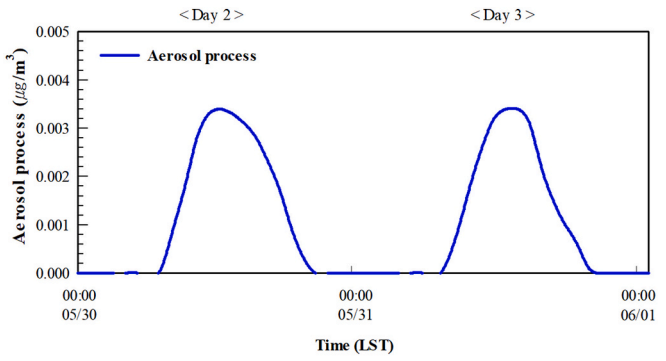

Fig. 10. Time series of differences between SO_4^{2-}concentrations on Day 2 (May 29) and Day 3 (May 30), when sulfate (SO_4^{2-}) concentrations increased because of the "aerosol process" in the YS region (the OCEAN case minus the BASE case). More SO_4^{2-} formed in the YS region in the OCEAN case because of marine emissions.

reaction by OH, similar to the findings in the BASE case, suggesting that even if ocean emissions are included, the mechanism of SO_4^{2-} formation over the Yellow Sea does not significantly change and that concentrations of SO_4^{2-} are subject to change, depending on changes in the amounts of emissions.

Fig. 11 shows the distributions of SO_4^{2-} concentrations that changed as a result of ocean emissions during the EP. On all case days (Days 1–4), SO_4^{2-} concentrations appeared to increase (0.25 $\mu g/m^3$ to 0.70 $\mu g/m^3$) in the sea area around South Korea. The difference between the results of the IPR analyses of the OCEAN and BASE cases and those of the STM analyses (not shown) indicated that the increases in SO_4^{2-} concentrations would mainly be attributed to the increased chemical production by the "aerosol process" because of the added ocean emissions, particularly SO_2. As seen in Fig. 11, the increased SO_4^{2-} concentrations and their distributions on each case day were not constant, but they varied, implying that increases in SO_4^{2-} concentrations caused by ocean emissions depend on the weather conditions associated with the chemical production, dispersion, and transport (especially wind speed and wind direction) of SO_4^{2-} and its precursors.

We wish to note here that the addition of ocean emissions does not simply lead to an increase in SO_4^{2-} concentrations. From the distribution of concentrations shown in Fig. 12, the difference between the results of the OCEAN and BASE case simulations showed increases in SO_4^{2-} concentrations (up to 4.79 $\mu g/m^3$) in most ocean areas circumjacent to South Korea, but decreases (up to −2.65 $\mu g/m^3$) in some areas of the South Sea and the East Sea. In regions where ocean emissions increased but SO_4^{2-} concentrations decreased, elucidating its mechanism is difficult. SO_2 could oxidize in the atmosphere and form sulfuric acid (H_2SO_4), and H_2SO_4 could react with NH_3 to form ammonium sulfate ($(NH_4)_2SO_4$). The NO_x could also oxidize in the atmosphere and generate nitric acid (HNO_3), and HNO_3 could react with NH_3 to form ammonium nitrate (NH_4NO_3). During this process, H_2SO_4 and HNO_3 are in a competitive relationship for NH_3; hence, the ratio among the three constituents is crucial to determining concentrations of SO_4^{2-}, NO_3^{2-}, and NH_4^+. Ocean emissions include those of not only SO_2 but also various substances such as NO_x and NH_3, and the type and amounts of air pollutants transported from the inland areas of South Korea to the ocean are not consistent. Furthermore, some substances contained in ocean emissions may affect the reduction of OH concentrations, which in turn may inhibit the chemical production of SO_4^{2-}.

Thus, to accurately interpret changes in SO_4^{2-} concentrations that

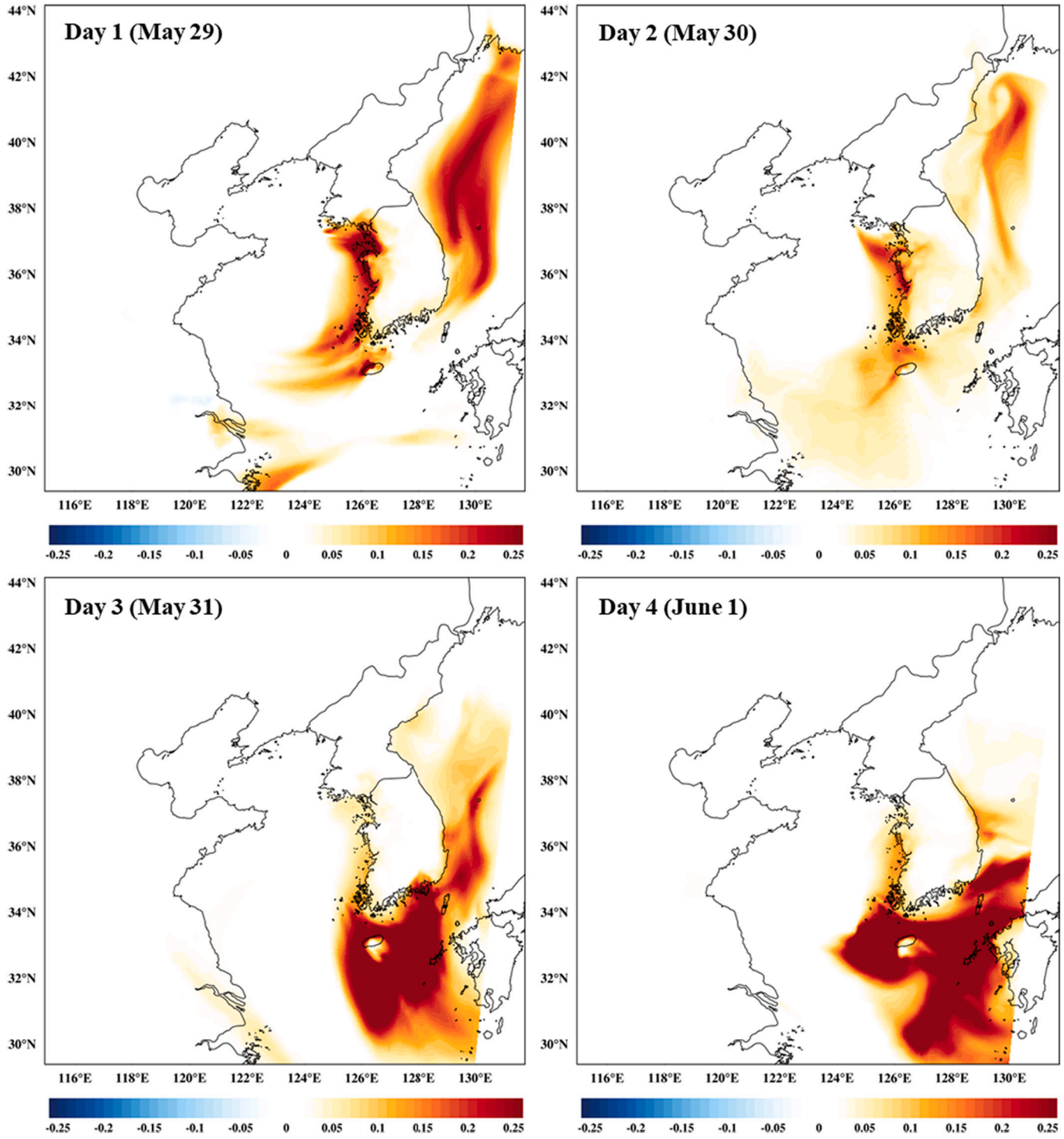

Fig. 11. The distribution of differences between SO_4^{2-} concentrations of OCEAN case and those of the BASE case during the EP (May 29–June 1). Each value represents the daily average of the grid values.

account for ocean emission will require an accurate analysis of the non-linear chemical reactions among these constituents. As such a process would entail a complicated and time-consuming effort, it should be investigated as an independent research topic in future work. The results of this study have confirmed that concentrations of SO_4^{2-} on the sea surface do not increase simply proportional to the amounts and the distribution of ocean emissions. In fact, because of complicated non-linear chemical reactions, concentrations could decrease in some areas.

On the basis of the analytical results presented above, the primary mechanism of SO_4^{2-} formation over the Yellow Sea (i.e., $OH + SO_2 \rightarrow H_2SO_4 + HO_2$) changed only slightly when we accounted for ocean emissions; nevertheless, we identified both increases and decreases in SO_4^{2-} concentrations depending on changes in emissions. Unfortunately, the range of ocean emissions data analyzed in this study was limited to the ocean circumjacent to South Korea. That is, the study did not analyze ocean emissions over the entirety of the Yellow Sea. An investigation of the ocean emissions data covering the entire Yellow Sea, including marine areas circumjacent to China, would more precisely explain the

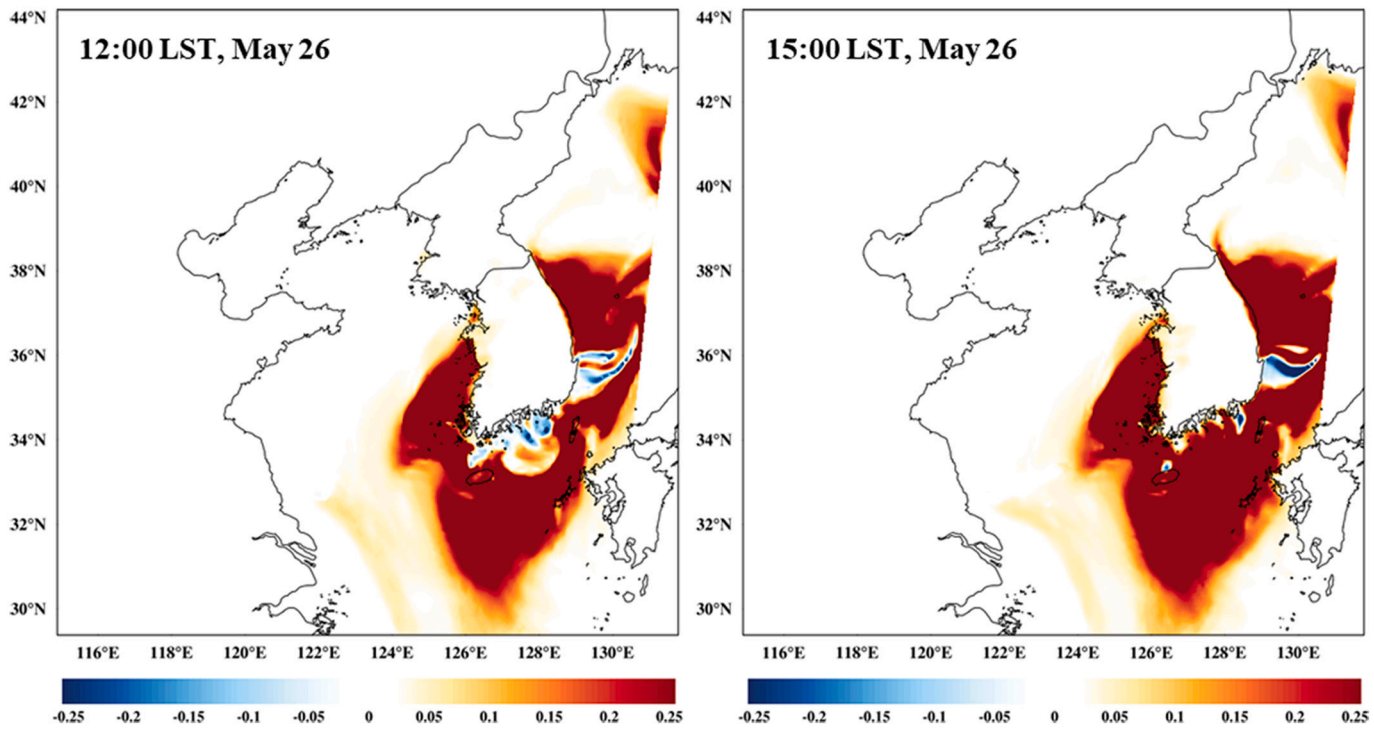

Fig. 12. Horizontal distributions of difference between SO_4^{2-} concentrations of the OCEAN case and those of the BASE case at 12:00 and 15:00 LST 26 May.

mechanism of SO_4^{2-} formation over the Yellow Sea. Furthermore, this study found regions where SO_4^{2-} concentrations decreased despite the addition of ocean emissions, which calls for further research that comprehensively interprets changes in aerosol concentrations at the sea surface due to ocean emissions.

4. Summary and conclusion

This study quantitatively analyzed chemical changes taking place in the high-concentration SO_4^{2-} phenomenon that occurred at the surface of the Yellow Sea caused by the long-range transport of air pollutants. For the analysis, we applied a three-dimensional photochemical model, the Community Multi-scale Air Quality (CMAQ), to carry out an air quality simulation during the 2016 Korea-United States Air Quality (KORUS-AQ) period. Using surface $PM_{2.5}$ observation data from China and South Korea together with the DC-8 aircraft measurement data of some areas of the Yellow Sea, we extensively evaluated CMAQ simulation results.

From the distribution of concentrations of $PM_{2.5}$ constituents (i.e., SO_4^{2-}, NO_3^-, NO_4^+, elemental carbon, primary organic carbon, and secondary organic carbon) simulated by CMAQ, we identified high concentrations of these constituents centering around eastern China, the Liaodong Peninsula, and the western inland areas of the Korean Peninsula. Interestingly, however, the distribution of SO_4^{2-} concentrations as high as (14.44 $\mu g/m^3$) showed characteristics that distinctly differed from those of the other constituents. Although emissions at the surface of the Yellow Sea are limited compared to those over land, the simulation showed high concentrations of SO_4^{2-} over the sea. To analyze this phenomenon in detail, we selected the period from May 29 to June 1, when high concentrations of SO_4^{2-} over the Yellow Sea were most apparent and identified the production and loss processes of chemical SO_4^{2-} in the Yellow Sea region (YS), in which the formation of the high concentration SO_4^{2-} occurred.

From the results of the IPR analysis, on May 29 (Day 1, the first case day), we found an increased concentration of SO_4^{2-} resulting from "horizontal transport" over the Yellow Sea; and on May 30 and 31 (Days 2 and 3, the second and third case days), we found an increase resulting from the "aerosol process". The formation of SO_4^{2-} resulting from the "aerosol process" was the result of the oxidation of SO_2 transported through eastern China, the Liaodong Peninsula, and the western area of the Korean Peninsula by OH on the sea surface. We found that the formation of SO_4^{2-} on each case day differed depending on both weather conditions and the distribution of SO_2 and OH concentrations.

To investigate changes in the production and loss of SO_4^{2-} over the Yellow Sea when we accounted for ocean emissions, we conducted additional modeling that accounted for ocean emissions (the OCEAN case) and compared the results with those of the BASE case. From the results of the IPR analysis of the OCEAN case, we confirmed that the mechanism of SO_4^{2-} formation over the Yellow Sea was not significantly affected by the addition of ocean emissions. We also found that the increases and decreases in SO_4^{2-} concentrations depended on whether or not ocean emissions were taken into account. When they were, concentrations of SO_4^{2-} increased in most marine areas circumjacent to South Korea but decreased in some areas. These results indicate that concentrations of SO_4^{2-} do not increase simply proportional to the amounts and distribution of ocean emissions but that they could decrease in some regions because of complex non-linear chemical reactions.

From the results of this study, we found that the formation of chemical SO_4^{2-} over the Yellow Sea occurs not only in the winter but also in the spring (KORUS-AQ period) and that the inflow path of SO_2 to the Yellow Sea is not always constant but instead differs according to seasonal pressure patterns. When we accounted for ocean emissions, we identified only a slight change in the mechanism of SO_4^{2-} formation over the Yellow Sea; on the other hand, we found an increase in SO_4^{2-} concentrations at the sea surface owing to an increase of emissions. Despite the addition of ocean emissions in this study, concentrations of SO_4^{2-} decreased in some regions, which calls for additional research that accurately interprets this phenomenon.

Declaration of Competing Interest

The authors declare that they have no known competing financial interests or personal relationships that could have appeared to influence

the work reported in this paper.

Acknowledgments

This research was partially supported by the Basic Science Research Program through the National Research Foundation of Korea (NRF) funded by the Ministry of Science and Technology (NRF-2019R1C1C1003428) and the Basic Science Research Program through the National Research Foundation of Korea (NRF) funded by the Ministry of Education (NRF-2020R1A6A1A03044834).

Appendix A. Supplementary data

Supplementary data to this article can be found online at https://doi.org/10.1016/j.atmosres.2021.105756.

References

Bae, C., Kim, B.U., Kim, H.C., Yoo, C., Kim, S., 2020a. Long-range transport influence on key chemical components of PM2.5 in the Seoul metropolitan area, South Korea, during the years 2012-2016. Atmosphere (Basel). https://doi.org/10.3390/ATMOS11010048.

Bae, M., Kim, B.U., Kim, H.C., Kim, S., 2020b. A multiscale tiered approach to quantify contributions: a case study of PM2.5 in South Korea during 2010-2017. Atmosphere (Basel). 11, 5–15. https://doi.org/10.3390/atmos11020141.

Boylan, J.W., Russell, A.G., 2006. PM and light extinction model performance metrics, goals, and criteria for three-dimensional air quality models. Atmos. Environ. 40, 4946–4959. https://doi.org/10.1016/j.atmosenv.2005.09.087.

Byun, D., Schere, K.L., 2006. Review of the governing equations, computational algorithms, and other components of the Models-3 Community Multiscale Air Quality (CMAQ) modeling system. Appl. Mech. Rev. 59, 51–77.

Cha, J.W., Shin, B., Ko, H.J., Lim, Y.K., Ryoo, S.B., 2020. Water-Soluble Ionic Characteristics of Aerosols in the Marine Boundary Layer over the Yellow Sea during the KORUS-AQ Campaign. Asia-Pacific J. Atmos. Sci. 56, 467–483. https://doi.org/10.1007/s13143-019-00151-8.

Emery, C., Liu, Z., Russell, A.G., Odman, M.T., Yarwood, G., Kumar, N., 2017. Recommendations on statistics and benchmarks to assess photochemical model performance. J. Air Waste Manage. Assoc. 67, 582–598. https://doi.org/10.1080/10962247.2016.1265027.

Fan, Q., Lan, J., Liu, Yiming, Wang, X., Chan, P., Hong, Y., Feng, Y., Liu, Yexin, Zeng, Y., Liang, G., 2015. Process analysis of regional aerosol pollution during spring in the Pearl River Delta region. China. Atmos. Environ. 122, 829–838. https://doi.org/10.1016/j.atmosenv.2015.09.013.

Guan, D., Su, X., Zhang, Q., Peters, G.P., Liu, Z., Lei, Y., He, K., 2014. The socioeconomic drivers of China's primary PM2.5 emissions. Environ. Res. Lett. 9 https://doi.org/10.1088/1748-9326/9/2/024010.

Ho, K.F., Lee, S.C., Chan, C.K., Yu, J.C., Chow, J.C., Yao, X.H., 2003. Characterization of chemical species in PM2.5 and PM10 aerosols in Hong Kong. Atmos. Environ. 37, 31–39. https://doi.org/10.1016/S1352-2310(02)00804-X.

Hurley, P.J., Blockley, A., Rayner, K., 2001. Verification of a prognostic meteorological and air pollution model for year-long predictions in the Kwinana industrial region of Western Australia. Atmos. Environ. 35, 1871–1880. https://doi.org/10.1016/S1352-2310(00)00486-6.

Itahashi, S., Uno, I., Kim, S., 2012. Source contributions of sulfate aerosol over East Asia estimated by CMAQ-DDM. Environ. Sci. Technol. 46, 6733–6741. https://doi.org/10.1021/es300887w.

Itahashi, S., Yamaji, K., Chatani, S., Hayami, H., 2018. Refinement of modeled aqueous-phase sulfate production via the fe- and Mn-catalyzed oxidation pathway. Atmosphere (Basel). 9, 1–17. https://doi.org/10.3390/atmos9040132.

Jeon, W., Choi, Y., Mun, J., Lee, S.H., Choi, H.J., Yoo, J.W., Lee, H.J., Lee, H.W., 2018. Behavior of sulfate on the sea surface during its transport from Eastern China to South Korea. Atmos. Environ. 186, 102–112. https://doi.org/10.1016/j.atmosenv.2018.05.017.

Jo, Y.J., Lee, H.J., Jo, H.Y., Woo, J.H., Kim, Y., Lee, T., Heo, G., Park, S.M., Jung, D., Park, J., Kim, C.H., 2020. Changes in inorganic aerosol compositions over the Yellow Sea area from impact of Chinese emissions mitigation. Atmos. Res. 240, 104948. https://doi.org/10.1016/j.atmosres.2020.104948.

Jung, J., Choi, Y., Wong, D.C., Nelson, D., Lee, S., 2021. Role of sea fog over the Yellow Sea on air quality with the direct effect of aerosols. J. Geophys. Res. Atmos. 126 https://doi.org/10.1029/2020JD033498 e2020JD033498.

Kim, B.G., Han, J.S., Park, S.U., 2001. Transport of SO2 and aerosol over the Yellow Sea. Atmos. Environ. 35, 727–737. https://doi.org/10.1016/S1352-2310(00)00344-7.

Kim, H.S., Chung, Y.S., Lee, S.G., 2012. Characteristics of aerosol types during large-scale transport of air pollution over the Yellow Sea region and at Cheongwon, Korea, in 2008. Environ. Monit. Assess. 184, 1973–1984. https://doi.org/10.1007/s10661-011-2092-9.

Kim, C.H., Kim, E., Bae, C., Cho, J.H., Kim, B.U., Kim, S., 2017. Regional contributions to particulate matter concentration in the Seoul metropolitan area, South Korea: Seasonal variation and sensitivity to meteorology and emissions inventory. Atmos. Chem. Phys. https://doi.org/10.5194/acp-17-10315-2017.

Lee, H.S., Kang, B.W., 2001. Chemical characteristics of principal PM2.5 species in Chongju, South Korea. Atmos. Environ. 35, 739–746. https://doi.org/10.1016/S1352-2310(00)00267-3.

Lee, H.S., Kang, C.M., Kang, B.W., Kim, H.K., 1999. Seasonal variations of acidic air pollutants in Seoul, South Korea. Atmos. Environ. 33, 3143–3152. https://doi.org/10.1016/S1352-2310(98)00382-3.

Lee, S.B., Bae, G.N., Moon, K.C., Kim, Y.P., 2002. Characteristics of TSP and PM2.5 measured at Tokchok Island in the Yellow Sea. Atmos. Environ. 36, 5427–5435. https://doi.org/10.1016/S1352-2310(02)00671-4.

Lee, T., Choi, J., Lee, G., Ahn, J., Park, J.S., Atwood, S.A., Schurman, M., Choi, Y., Chung, Y., Collett, J.L., 2015. Characterization of aerosol composition, concentrations, and sources at Baengnyeong Island, Korea using an aerosol mass spectrometer. Atmos. Environ. https://doi.org/10.1016/j.atmosenv.2015.08.038.

Li, L., Huang, C., Huang, H.Y., Wang, Y.J., Yan, R.S., Zhang, G.F., Zhou, M., Lou, S.R., Tao, S.K., Wang, H.L., Qiao, L.P., Chen, C.H., Streets, D.G., Fu, J.S., 2014. An integrated process rate analysis of a regional fine particulate matter episode over yangtze river delta in 2010. Atmos. Environ. 91, 60–70. https://doi.org/10.1016/j.atmosenv.2014.03.053.

Li, M., Zhang, Q., Kurokawa, J.I., Woo, J.H., He, K., Lu, Z., Ohara, T., Song, Y., Streets, D. G., Carmichael, G.R., Cheng, Y., Hong, C., Huo, H., Jiang, X., Kang, S., Liu, F., Su, H., Zheng, B., 2017. MIX: a mosaic Asian anthropogenic emission inventory under the international collaboration framework of the MICS-Asia and HTAP. Atmos. Chem. Phys. https://doi.org/10.5194/acp-17-935-2017.

Liu, T., Clegg, S.L., Abbatt, J.P.D., 2020a. Fast oxidation of sulfur dioxide by hydrogen peroxide in deliquesced aerosol particles. Proc. Natl. Acad. Sci. 117, 1354–1359. https://doi.org/10.1073/pnas.1916401117.

Liu, P., Ye, C., Xue, C., Zhang, C., Mu, Y., Sun, X., 2020b. Formation mechanisms of atmospheric nitrate and sulfate during the winter haze pollution periods in Beijing: Gas-phase, heterogeneous and aqueous-phase chemistry. Atmos. Chem. Phys. https://doi.org/10.5194/acp-20-4153-2020.

National Institute of Environmental Research (NIER) (2019) 2016 national air pollutant emissions, http://airemiss.nier.go.kr/user/boardList.do?command=view&page=1&board Id=74&boardSeq=526&id=airemiss_040100000000.

Pan, S., Choi, Y., Roy, A., Li, X., Jeon, W., Souri, A.H., 2015. Modeling the uncertainty of several VOC and its impact on simulated VOC and ozone in Houston. Texas. Atmos. Environ. 120, 404–416. https://doi.org/10.1016/j.atmosenv.2015.09.029.

Pan, S., Choi, Y., Roy, A., Jeon, W., 2017. Allocating emissions to 4 km and 1 km horizontal spatial resolutions and its impact on simulated NOx and O3 in Houston. TX. Atmos. Environ. 164, 398–415. https://doi.org/10.1016/j.atmosenv.2017.06.026.

Park, S.M., Song, I.H., Park, J.S., Oh, J., Moon, K.J., Shin, H.J., Ahn, J.Y., Do Lee, M., Kim, J., Lee, G., 2018. Variation of PM2.5 chemical compositions and their contributions to light extinction in Seoul. Aerosol Air Qual. Res. 18, 2220–2229. https://doi.org/10.4209/aaqr.2017.10.0369.

Peterson, D.A., Hyer, E.J., Han, S.O., Crawford, J.H., Park, R.J., Holz, R., Kuehn, R.E., Eloranta, E., Knote, C., Jordan, C.E., Lefer, B.L., 2019. Meteorology influencing springtime air quality, pollution transport, and visibility in Korea. Elementa 7. https://doi.org/10.1525/elementa.395.

Pozzoli, L., Janssens-Maenhout, G., Diehl, T., Bey, I., Schultz, M.G., Feichter, J., Vignati, E., Dentener, F., 2011. Re-analysis of tropospheric sulfate aerosol and ozone for the period 1980-2005 using the aerosol-chemistry-climate model ECHAM5-HAMMOZ. Atmos. Chem. Phys. 11, 9563–9594. https://doi.org/10.5194/acp-11-9563-2011.

Requia, W.J., Jhun, I., Coull, B.A., Koutrakis, P., 2019. Climate impact on ambient PM2.5 elemental concentration in the United States: a trend analysis over the last 30 years. Environ. Int. 131, 104888. https://doi.org/10.1016/j.envint.2019.05.082.

Simpson, I.J., Blake, D.R., Blake, N.J., Meinardi, S., Barletta, B., Hughes, S.C., Fleming, L. T., Crawford, J.H., Diskin, G.S., Emmons, L.K., Fried, A., Guo, H., Peterson, D.A., Wisthaler, A., Woo, J.-H., Barré, J., Gaubert, B., Kim, J., Kim, M.J., Kim, Y., Knote, C., Mikoviny, T., Pusede, S.E., Schroeder, J.R., Wang, Y., Wennberg, P.O., Zeng, L., 2020. Characterization, sources and reactivity of volatile organic compounds (VOCs) in Seoul and surrounding regions during KORUS-AQ. Elem. Sci. Anthr. 8 https://doi.org/10.1525/elementa.434.

Skamarock, W.C., Klemp, J.B., 2008. A time-split nonhydrostatic atmospheric model for weather research and forecasting applications. J. Comput. Phys. 227, 3465–3485. https://doi.org/10.1016/j.jcp.2007.01.037.

Souri, Amir H., Choi, Y., Jeon, W., Kochanski, A.K., Diao, L., Mandel, J., Bhave, P.V., Pan, S., 2017a. Quantifying the Impact of Biomass burning Emissions on Major Inorganic Aerosols and their Precursors in the U.S. J. Geophys. Res. Atmos. 122, 12,020–12,041. https://doi.org/10.1002/2017JD026788.

Souri, Amir Hossein, Choi, Y., Jeon, W., Woo, J.H., Zhang, Q., Kurokawa, J.I., 2017b. Remote sensing evidence of decadal changes in major tropospheric ozone precursors over East Asia. J. Geophys. Res. 122, 2474–2492. https://doi.org/10.1002/2016JD025663.

Wang, W., Liu, M., Wang, T., et al., 2021. Sulfate formation is dominated by manganese-catalyzed oxidation of SO_2 on aerosol surfaces during haze events. Nat. Commun. 12, 1993. https://doi.org/10.1038/s41467-021-22091-6.

Willmott, C.J., Ackleson, S.G., Davis, R.E., Feddema, J.J., Klink, K.M., Legates, D.R., Odonnell, J., Rowe, C.M., 1985. Statistics for the evaluation and comparison of models. J. Geophy. Res. Oceans 90, 8995–9005. https://doi.org/10.1016/0198-0254(86)91285-9.

Zhang, H., Xu, Y., Jia, L., 2021. A chamber study of catalytic oxidation of SO_2 by Mn^{2+}/Fe^{3+} in aerosol water. Atmos. Environ. 245, 118019. https://doi.org/10.1016/j.atmosenv.2020.118019.